J. Math. Computer Sci., 36 (2025), 185–206

Online: ISSN 2008-949X

Journal of Mathematics and Computer Science

Journal Homepage: www.isr-publications.com/jmcs

Giardiasis transmission dynamics: insights from fractal-fractional modeling and deep neural networks

M. A. El-Shorbagy[a,b], Saira Tabussam[c], Mati ur Rahman[d,e,*], Waseem[f]

[a]Department of Mathematics, College of Science and Humanities in Al-Kharj, Prince Sattam bin Abdulaziz University, Al-Kharj 11942, Saudi Arabia.

[b]Department of Basic Engineering Science, Faculty of Engineering, Menoufia University, Shebin El-Kom 32511, Egypt.

[c]Department of Applied Sciences, National Textile University, Faisalabad 37610, Pakistan.

[d]School of Mathematical Sciences, Jiangsu University, Zhenjiang 212013, Jiangsu, P.R. China.

[e]Department of computer science and mathematics, Lebanese American university, Beirut, Lebanon.

[f]School of Mechnical Engineering, Jiangsu University, Zhenjiang 212013, Jiangsu, P.R. China.

Abstract

The World Health Organization highlights Giardias as a neglected zoonotic disease caused by Giardia duodenalis. The disease often goes overlooked despite the significant harm it causes humans and animals. We present a mathematical model for transmitting Giardiasis incorporating various preventative measures, including screening, treatment, and environmental sanitation. Among the factors influencing Giardiasis transmission within a community is the interaction parameter between humans and the environment. In this manuscript, Atangana-Baleanu Caputo (ABC) derivatives of fractional order v and fractal dimension q are utilized to explore a modified model with a fractal-fractional approach. The study qualitatively analyses the model using functional non-linearity and population-based fixed-point theory. The fractional Adams-Bashforth iterative method is used to obtain numerical solutions. Ulam-Hyers (UH) stability techniques are used to analyze stability in this study. A comparison is made between simulation results for all compartments and Giardia duodenalis data already available. To manage Giardiasis duodenalis effectively, societal behavioral changes and adherence to preventive measures are essential to controlling the effective transmission rate. Additionally, a deep neural network (DNN) approach is used to analyze the given disease condition with excellent accuracy in training, testing, and validation data.

Keywords: Giardiasis duodenalis, existence result, fractal-fractional ABC operator, deep neural network, numerical results.

2020 MSC: 34K37, 92D30, 65L05, 34A08.

1. Introduction

Children under five are particularly vulnerable to Giardiasis, caused by the Giardia lamblia parasite, also known as Giardia intestinalis or Giardia duodenalis. Giardia begins its life cycle when cysts are in-

*Corresponding author
Email address: MatiUr.Rahman@lau.edu.lb (Mati ur Rahman)

doi: 10.22436/jmcs.036.02.04

Received: 2024-02-20 *Revised:* 2024-05-14 *Accepted:* 2024-05-29

gested from food or water that the feces of an infected host have contaminated [13]. Water and sanitation practices are inadequate when preparing food, exacerbating diarrhea transmission. Giardiasis can start in the community with just ten cysts released by an infected individual in their excretion [9, 36].

Only A and B of the eight gene groups harm humans regarding Giardiasis. Animals are primarily infected by genotypes C to H. Diarrhea, nutrient malabsorption, cognitive impairment, defects in development, fever, itchiness, weight loss, stomach cramps, floating greasy poop, upset stomach, and nausea are some common symptoms. The parasite affects both economically and developmentally developed countries, although its effects are greater in the latter [37]. Giardiasis was designated an Ignored Disease Initiative by the World Health Organization Since September 2004, it has been associated with poverty and high burdens. In a given year, Giardiasis is estimated to affect 2.80 billion people worldwide. Development countries lack safe drinking water and sanitation, which causes many people to exhibit Giardiasis symptoms. Since remote communities, inadequate transportation, a shortage of qualified health workers, as well as insufficient lab facilities for accurate diagnosis, contribute to the elevated prevalence of diseases in developing countries. Identifying, detecting, and reporting infectious diseases accurately is difficult due to the lack of qualified health workers and lab facilities [20, 24, 34, 41].

The risk of giardiasis contamination escalates with raw food consumption, leading to international recommendations for food safety practices. Among these are maintaining proper hand hygiene to prevent protozoan parasites, separating raw and cooked food, using purified or boiled water, and cooking food over 70 degrees Celsius. In conclusion, Giardiasis poses a significant global health concern, affecting millions, particularly in regions with inadequate sanitation and limited access to clean water. Efforts to combat the disease involve medical interventions and improvements in sanitation infrastructure, hygiene practices, and food safety measures [40]. We have made significant progress in mathematical modeling to understand better the epidemiology and dynamics of diseases such as giardiasis. An evaluation of disease dynamics based on giardiasis dynamics has been developed by Saul and Nyerere [37]. According to their findings, giardiasis dynamics depend heavily on transmission from person to person. Waters et al. [26] developed another model for simulating Giardia transmission dynamics in rural Australia. A study found that zoonotic protozoa can cause epidemic infections in humans despite the absence of transmission from humans to humans. It is evident from these findings that environmental reservoirs play a crucial role in transmitting transmissible zoonotic species. To study immunity to Giardia duodenalis secondary infections, Li et al. infected mice using a mouse model. A vaccine for giardiasis that is robust to reinfection can be developed using adult mouse models. Giardiasis continues to affect millions of people in impoverished nations despite countless studies examining the disease's dynamics. Evaluation of existing control measures is crucial to working towards eradicating this disease. Giardiasis dynamics have never been examined for screening, treatment, or sanitation interventions. Therefore, the present study aims to shed light on how screening, treatment, and sanitation affect giardiasis transmission dynamics.

$$\begin{cases} \dot{\mathbb{S}}(\xi) = \Lambda^* + \rho\mathbb{R} - (\beta_1^*\mathbb{I} + \beta_2^*\mathbb{A} + \beta_3^*\mathbb{G})\mathbb{S} - \mu^*\mathbb{S}, \\ \dot{\mathbb{E}}(\xi) = (\beta_1^*\mathbb{I} + \beta_2^*\mathbb{A} + \beta_3^*\mathbb{G})\mathbb{S} - (\mu^* + \kappa^*)\mathbb{E}, \\ \dot{\mathbb{I}}(\xi) = (1-\alpha^*)\kappa^*\mathbb{E} + \nu^*\mathbb{A} - (\eta^* + \psi^* + \mu^* + p^* + \sigma^*)\mathbb{I}, \\ \dot{\mathbb{A}}(\xi) = \alpha^*\kappa^*\mathbb{E} + \eta^*\mathbb{I} - (\mu^* + \nu^* + \delta^* + \gamma^*)\mathbb{A}, \\ \dot{\mathbb{R}}(\xi) = (p^* + \sigma^*)\mathbb{I} + \gamma^*\mathbb{A} - (\mu^* + \rho^*)\mathbb{R}, \\ \dot{\mathbb{G}}(\xi) = \varepsilon^*\mathbb{I} + d^*\mathbb{A} - (\tau^* + \chi^*)\mathbb{G}, \end{cases} \tag{1.1}$$

The list of parameters utilised in the model, as mentioned above, and their comprehensive descriptions are presented Table 1.

Table 1: Description of the parameters.

Parameters	Description
Λ^*	Human recruitment rates
ρ^*	Removing individuals with warnings
β_1^*	Transmission rate between susceptible and infected
τ^*	Pathogens in the environment that cause death
σ^*	Infectious individuals treated at a high rate
ψ^*	Human infection rates are low because of Giardiasis
β_2^*	Transmission rate between asymptomatic and susceptible individuals
β_3^*	Environmental and human transmission rate
p^*	Recoveries of infected individuals
δ^*	Giardiasis-related drought rate for asymptomatic humans
K^*	Saturating constant of the environment
κ^*	Incubation period for pathogens in humans
μ^*	Ratio of natural deaths in humans
α^*	Giardiasis infection probability
ϵ^*	Rate of Giardia shed into the environment by infected humans
d^*	Asymptomatic humans shed Giardia into the environment at a high rate
ν^*	Infectious state progression rate/screening rate of asymptomatic patients
γ^*	Asymptomatic humans' natural recovery rate
χ^*	Sanitation rate of the environment
η^*	The percentage of infected humans who become asymptomatic

We will revisit the model described in equation (1.1), adding a derivative of arbitrary order with $0 < v \leqslant 1$ and a fractal dimension with $0 < q \leqslant 1$,

$$\begin{cases} {}^{\mathcal{ABC}}\mathrm{D}_{\xi}^{v,q}\mathbb{S}(\xi) = \Lambda^* + \rho\mathbb{R} - (\beta_1^*\mathbb{I} + \beta_2^*\mathbb{A} + \beta_3^*\mathbb{G})\mathbb{S} - \mu^*\mathbb{S}, \\ {}^{\mathcal{ABC}}\mathrm{D}_{\xi}^{v,q}\mathbb{E}(\xi) = (\beta_1^*\mathbb{I} + \beta_2^*\mathbb{A} + \beta_3^*\mathbb{G})\mathbb{S} - (\mu^* + \kappa^*)\mathbb{E}, \\ {}^{\mathcal{ABC}}\mathrm{D}_{\xi}^{v,q}\mathbb{I}(\xi) = (1-\alpha^*)\kappa^*\mathbb{E} + \nu^*\mathbb{A} - (\eta^* + \psi^* + \mu^* + p^* + \sigma^*)\mathbb{I}, \\ {}^{\mathcal{ABC}}\mathrm{D}_{\xi}^{v,q}\mathbb{A}(\xi) = \alpha^*\kappa^*\mathbb{E} + \eta^*\mathbb{I} - (\mu^* + \nu^* + \delta^* + \gamma^*)\mathbb{A}, \\ {}^{\mathcal{ABC}}\mathrm{D}_{\xi}^{v,q}\mathbb{R}(\xi) = (p^* + \sigma^*)\mathbb{I} + \gamma^*\mathbb{A} - (\mu^* + \rho^*)\mathbb{R}, \\ {}^{\mathcal{ABC}}\mathrm{D}_{\xi}^{v,q}\mathbb{G}(\xi) = \varepsilon^*\mathbb{I} + d^*\mathbb{A} - (\tau^* + \chi^*)\mathbb{G}, \\ \mathbb{S}(0) = \mathbb{S}_0 \geqslant 0, \quad \mathbb{E}(0) = \mathbb{E}_0 \geqslant 0, \quad \mathbb{I}(0) = \mathbb{I}_0 \geqslant 0, \quad \mathbb{A}(0) = \mathbb{A}_0 \geqslant 0, \\ \mathbb{R}(0) = \mathbb{R}_0 \geqslant 0, \quad \mathbb{G}(0) = \mathbb{G}_0 \geqslant 0, \quad 0 < v, q \leqslant 1. \end{cases} \tag{1.2}$$

We analyses the above equation (1.2) in the sense of ABC fractal-fractional order derivative. This method yields more realistic results with more versatility than integer-order derivatives. We examine equation (1.2), which represents a situation that falls between two integer values and has fractional order v and fractal dimension q. The whole compartment density should rapidly converge at lower orders in the result.

The fractal fractional order differential equation transforms both the order and the dimension of the system into rational values by transforming them each into a rational value according to the fractal-fractional order differential equation. A differential equation with this property can be generalized to any derivative order and dimension. Fractal-fractional operators were introduced by Atangana in [4], which established the relationship between fractional and fractal calculus. Numerous researchers applied fractal-fractional operators to different linear and nonlinear mathematical disease model [5, 22, 28, 29]. Since modern calculus differs from classical calculus in this way, there has been a heightened interest in it. By using fractional global operators, fractional calculus can provide a high degree of freedom for modelling physical and biological problems. Consequently, scholars of fractional calculus have proposed numerous documents and articles [16, 30]. Researchers present their theoretical and numerical analysis of

non-integer-order differential and integral equations in several books and monographs [6, 17, 19, 27, 38]. As discussed in [21], several researchers have applied various methods to solve differential equations for Giardiasis transmission.

In modern calculus, rational and complex numbers are used to extend the traditional integration and differentiation rules, allowing us to apply it to situations between integer order, fractional and fractal-fractional orders as described in [12, 32, 33]. Integer-order differential equations have been used to model many real-life problems, including population models, logistic population models, HIV, SEIR, TB, cancer models, predator-prey models, and others. As seen in [35, 39, 43], there has been a significant improvement in numerical solutions to these equations as a result of converting them to arbitrary-order differential equations. Some scholars have used to apply Banach contraction theorems, fixed-point theory, topological degree theories, and the Leray-Schauder theorem [2, 3, 8, 14, 18].

Despite being known to scientists since the 1940s [23], artificial neural networks (ANNs) have not gained enough traction because of computing equipment' capabilities. Because of their complicated design, ANNs have become a strong computational paradigm. Artificial neural networks have developed into information-processing systems that resemble biological neural networks in certain aspects of performance because to advancements in computer processing and data storage [31]. Their capacity to retain and retrieve patterns, demonstrate associative memory, and resolve optimization issues helped them become well-known. Many studies have been carried out to improve knowledge of HNNs, investigate their theoretical characteristics, and create effective learning algorithms throughout time [7]. An ANN design consists of three layers: input, hidden, and output, where neurons are housed. A deep neural network (DNN) is referred to as such when it has numerous hidden layers [15]. ANNs are widely used in the solution of dynamic systems, such as ODE-modeled systems. The relevance of ANNs is found in their flexibility to various dynamic systems, an area in which traditional numerical techniques have benefits and drawbacks in terms of stability, accuracy, and convergence. An innovative method employs neural networks to parameterize hidden states effectively across diverse problem-solving scenarios [10]. The Ordinary Differential Equation Variational Auto-Encoder (ODE2VAE) excels in handling complex sequential data and latent dynamics [42]. A groundbreaking algorithm identifies multiple solutions to ODEs, offering valuable insights into complex problem-solving [11]. Neural networks, which tackle nonlinear differential equations, offer a potent framework for challenging mathematical issues.

Researchers used FDEs to optimize and approximate solutions due to their inherent difficulty finding the exact solutions. Various methods have been used to solve numerical problems, including modified Euler techniques, Taylor's series method, Adams-Bashforth techniques, predictor-corrector methods, integral transforms, and wavelet methods. As a result of these considerations, the proposed model is studied under fractal-fractional operator in the sense of ABC. By using the concept of fixed-point theory we analyze the existence and uniqueness of solution. For the stability of of the model we applied the Ulam-Hyers stability approach. To find the approximate solution, we developed the Adams-Bashforth technique for the considered model. Furthermore, the novel approach of deep neural network is analyzed and better results for the proposed model under consideration are obtained. These given solution is trained well and the obtained figures shows best performance of the used technique.

For the limitation of the proposed study, it is imperative to acknowledge several key constraints. Firstly, while the fractal-fractional modeling and deep neural networks offer valuable insights, they rely on certain assumptions that may oversimplify the complex dynamics of giardiasis transmission. Secondly, the availability and quality of data could influence the accuracy and generalizability of the findings, potentially limiting their applicability to diverse populations or environmental settings. Furthermore, the lack of robust validation against independent datasets raises concerns about the reliability of the models. Additionally, ethical considerations surrounding the use of deep neural networks should be addressed, along with potential biases introduced by the modeling approach.

This paper is structured asfollows. The primary results are presented in Section 2. The model existence results and uniqueness of solution is presented in Section 3, as well as the Ulam-Hyers stability. The numerical solution of the system is obtained in Section 4. Deep neural network approach is used for

graphical illustration of the proposed model in section 5. Finally, we concluded our work in Section 6.

2. Fundamental results

Definition 2.1 ([4]). A continuously defined function $\mathcal{Z}(\xi)$ over the interval (a, b), characterized as a fractal dimension $0 < q \leqslant 1$ and a fractional order $0 < v \leqslant 1$ is formally defined in the sense of $\mathcal{ABC}$ as follows:

$$^{\mathcal{ABC}}\mathrm{D}^{v,q}(\mathcal{Z}(\xi)) = \frac{\mathcal{ABC}(v)}{1-v}\frac{d}{ds^q}\int_0^{\xi}\mathcal{Z}(s)_v\left[\frac{-\sigma}{1-v}\left(\xi - sv\right)^v\right]ds.$$

Hence, $\mathcal{ABC}(0) = \mathcal{ABC}(1) = 1$ is the normalization constant.

Definition 2.2 ([4]). A continuous function $\mathcal{Z}(\xi)$ over the interval (a, b), characterized by a fractal dimension $0 < q \leqslant 1$ and fractional order $0 < v \leqslant 1$, can be formally defined as follows within a framework of $\mathcal{ABC}$ as follows:

$$^{\mathcal{ABC}}\mathrm{I}_0^v(\mathcal{Z}(\xi)) = \frac{1-v}{\mathcal{ABC}(v)}\xi^{q-1}\mathcal{Z}(\xi) + \frac{qv}{\mathcal{ABC}(v)\Gamma(v)}\int_0^{\xi}(t-s)^{v-1}s^{q-1}\mathcal{Z}(s)ds.$$

Lemma 2.3 ([1]). *The solution for the given problem, considering values within the range of* $0 < v, q \leqslant 1$.

$$^{\mathcal{ABC}}D_0^v\mathcal{Z}(\xi) = q\xi^{q-1}\mathbb{V}(\xi, \mathcal{Z}(\xi)),\ \xi \in [0, T], \qquad \mathcal{Z}(0) = \mathcal{Z}_0,\ \ 0 < v, q \leqslant 1,$$

is provided by

$$\mathcal{Z}(\xi) = \mathcal{Z}_0 + \frac{(1-v)}{\mathcal{ABC}(v)}t^{q-1}\mathbb{V}(\xi, \mathcal{Z}(\xi)) + \frac{qv}{\Gamma(v)\mathcal{ABC}(v)}\int_0^{\xi}(t-s)^{v-1}s^{r-1}\mathbb{V}(s, \mathcal{Z}(s))ds.$$

Note: The Banach space is defined as follows to demonstrate the existence and uniqueness of the considered system as

$$\mathcal{Z} = \mathbb{V} = H([0, T] \times \mathbb{R}^6, \mathbb{R}),$$

where $\mathbb{V} = H[0, T]$ and the space norm is

$$\|W\| = \|\mathcal{Z}\| = \max_{t\in[0,T]}[|\mathbb{S}(\xi)| + |\mathbb{E}(\xi)| + |\mathbb{I}(\xi)| + |\mathbb{A}(\xi)| + |(\mathbb{R}(\xi)| + |(\mathbb{G}(\xi)|].$$

We introduce a fixed-point theorem to present our upcoming results.

Theorem 2.4 ([25]). ***statement:*** *consider a subset* **E** *of the set of integers* **Z**, *which is convex. Now, let's examine two operators, showd as* $\mathbf{Y}_1$ *and* $\mathbf{Y}_2$,

1. $\mathbf{Y}_1(w) + \mathbf{Y}_2(w) \in \mathbf{E}$ *for every* $w \in \mathbf{E}$;
2. $\mathbf{Y}_1$ *represents contraction;*
3. $\mathbf{Y}_2$ *has a continuous and compact structure.*

Therefore the operator equation $\mathbf{Y}_1 w + \mathbf{Y}_2 w = w$, *has one or more than one solution.*

3. Qualitative analysis of model (1.2)

This section presents results regarding the existence, uniqueness, and stability of the considered system (1.2). To achieve this objective, it is necessary to assume that the integral in question is differentiable.

As a result, we express the considered model (1.2) as follows:

$$\begin{cases} {}^{\mathcal{ABC}}\mathrm{D}^{v}(\mathbb{S}(\xi)) = q\xi^{q-1}(\mathcal{M}_1(\mathbb{S}(\xi),\xi) = \Lambda^* + \rho\mathbb{R} - (\beta_1^*\mathbb{I} + \beta_2^*\mathbb{A} + \beta_3^*\mathbb{G})\mathbb{S} - \mu^*\mathbb{S}, \\ {}^{\mathcal{ABC}}\mathrm{D}^{v}(\mathbb{E}(\xi)) = q\xi^{q-1}(\mathcal{M}_2(\mathbb{E}(\xi),\xi) = (\beta_1^*\mathbb{I} + \beta_2^*\mathbb{A} + \beta_3^*\mathbb{G})\mathbb{S} - (\mu^* + \kappa^*)\mathbb{E}, \\ {}^{\mathcal{ABC}}\mathrm{D}^{v}(\mathbb{I}(\xi)) = q\xi^{q-1}(\mathcal{M}_3(\mathbb{I}(\xi),t) = (1-\alpha^*)\kappa^*\mathbb{E} + \nu^*\mathbb{A} - (\eta^* + \psi^* + \mu^* + p^* + \sigma^*)\mathbb{I}, \\ {}^{\mathcal{ABC}}\mathrm{D}^{v}(\mathbb{A}(\xi)) = q\xi^{q-1}(\mathcal{M}_4(\mathbb{A}(\xi),\xi) = \alpha^*\kappa^*\mathbb{E} + \eta^*\mathbb{I} - (\mu^* + \nu^* + \delta^* + \gamma^*)\mathbb{A}, \\ {}^{\mathcal{ABC}}\mathrm{D}^{v}((\mathbb{R}(\xi)) = q\xi^{q-1}(\mathcal{M}_5((\mathbb{R}(\xi),\xi) = (p^* + \sigma^*)\mathbb{I} + \gamma^*\mathbb{A} - (\mu^* + \rho^*)\mathbb{R}, \\ {}^{\mathcal{ABC}}\mathrm{D}^{v}((\mathbb{G}(\xi)) = q\xi^{q-1}(\mathcal{M}_6((\mathbb{G}(\xi),\xi) = \varepsilon^*\mathbb{I} + d^*\mathbb{A} - (\tau^* + \chi^*)\mathbb{G}. \end{cases} \tag{3.1}$$

In view of (3.1) and for $\xi \in \mathcal{Z}$, then we have

$${}^{\mathcal{ABC}}\mathrm{D}_0^{v}\mathcal{Z}(\xi) = q\xi^{q-1}\mathbb{V}(\xi,\mathcal{Z}(\xi)),\ \xi \in [0,T], \qquad \mathcal{Z}(0) = \mathcal{Z}_0,\ \ 0 < v, q \leqslant 1,$$

with solution

$$\mathcal{Z}(\xi) = \mathcal{Z}_0 + \frac{(1-v)}{\mathcal{ABC}(v)}\xi^{q-1}\mathbb{V}(\xi,\mathcal{Z}(\xi)) + \frac{qv}{\Gamma(v)\mathcal{ABC}(v)}\int_0^{\xi}(\xi-s)^{v-1}s^{q-1}\mathbb{V}(s,\mathcal{Z}(s))ds, \tag{3.2}$$

where

$$\begin{cases} \mathcal{Z}(\xi) = \Big(\mathbb{S},\mathbb{E},\mathbb{I},\mathbb{A},\mathbb{R},\mathbb{G}\Big)^{T}, \\ \mathcal{Z}_0(t) = \Big(\mathbb{S}_0,\mathbb{E}_0,\mathbb{I}_0,\mathbb{A}_0,\mathbb{R}_0,\mathbb{G}_0,\Big)^{T}, \\ \mathbb{V}(\xi,\mathcal{Z}(\xi)) = \Big(\mathcal{G}_k(\mathbb{S},\mathbb{E},\mathbb{I},\mathbb{A},\mathbb{R},\mathbb{G},\xi)\Big)^{T},\ \ k = 1,2,3,\ldots,6. \end{cases}$$

Now, let's transform the system (1.2) into a fixed-point form. We introduce a mapping $\mathscr{T} : \mathbf{Y} \to \mathbf{Y}$ defined as follows:

$$\mathscr{T}\mathcal{Z}(\xi) = \mathcal{Z}_0 + \frac{(1-v)}{\mathcal{ABC}(v)}t^{q-1}\mathbb{V}(\xi,\mathcal{Z}(\xi)) + \frac{qv}{\Gamma(v)\mathcal{ABC}(v)}\int_0^{\xi}(t-s)^{v-1}s^{q-1}\mathbb{V}(s,\mathcal{Z}(s))ds.$$

Assume

$$\mathscr{T} = \mathbf{F} + \mathbf{H},$$

where

$$\mathbf{F}(\mathcal{Z}) = \mathcal{Z}_0(\xi) + \frac{(1-v)}{\mathcal{ABC}(v)}\xi^{q-1}\Big[\mathbb{V}(\xi,\mathcal{Z}(\xi))\Big],\quad \mathbf{H}(\mathcal{Z}) = \frac{qv}{\mathcal{ABC}(v)\Gamma(v)}\int_0^{\xi}(t-s)^{v-1}s^{q-1}\mathbb{V}(s,\mathcal{Z}(s))ds. \tag{3.3}$$

The next step will involve applying fixed-point theory to the given system.

(J1) There will be a constants $\mathscr{X}_{\mathbb{V}}, \mathscr{V}_{\mathbb{V}}, \ni |\mathbb{V}(\xi,\mathcal{Z}(\xi))| \leqslant \mathscr{X}_{\mathbb{V}}|\mathcal{Z}| + \mathscr{V}_{\mathbb{V}}$.

(J2) $\exists$ a constants $\mathbb{L}_{\mathbb{V}} > 0 \ni$ for every $\mathcal{Z}, \bar{\mathcal{Z}} \in \mathcal{Z}$ as $|\mathbb{V}(\xi,\mathcal{Z}) - \mathbb{V}(\xi,\bar{\mathcal{Z}})| \leqslant \mathbb{L}_{\mathbb{V}}[|\mathcal{Z}| - \bar{\mathcal{Z}}|]$.

Theorem 3.1. *If conditions* (J1) *and* (J2) *ensure that the system* (3.2) *possesses at least one solution, then the system* (1.2) *will have an equivalent number of solutions if the inequality* $\frac{(1-v)}{\mathcal{ABC}(v)}\xi^{q-1}\mathbb{L}_{\mathbb{V}} < 1$ *is satisfied.*

Proof. We have demonstrated the theorem through a two-step proof.

Step I: Suppose $\bar{\mathcal{Z}} \in \mathbf{E}$, and $\mathbf{E} = \mathcal{Z} \in \mathcal{Z} : |\mathcal{Z}| \leqslant \phi, \phi > 0$ is a convex closed set. According to (3.3), we can express the operator $\mathbf{Y}$ as follows:

$$\|\mathbf{F}(\mathcal{Z}) - \mathbf{F}(\bar{\mathcal{Z}})\| = \frac{(1-v)}{\mathcal{ABC}(v)}\xi^{q-1}\max_{\xi\in[0,\omega]}\Big|\mathbb{V}(\xi,\mathcal{Z}(\xi)) - \mathbb{V}(\xi,\bar{\mathcal{Z}}(\xi))\Big| \leqslant \frac{(1-v)}{\mathcal{ABC}(v)}\xi^{q-1}\mathbb{L}_{\mathbb{V}}\|\mathcal{Z} - \bar{\mathcal{Z}}\|.$$

Consequently, there is a contraction in the operator $\mathbf{Y}$.

Step-II: Now we need to demonstrate that **H** is bounded and continuous in a comparative sense. Since $\mathbb{V}$ is continuous, the operator **H** is defined over the entire domain. Furthermore, for $\mathcal{Z} \in \mathbf{E}$, the expression is as follows:

$$\begin{aligned}\|\mathbf{H}(\mathcal{Z})\| &= \max_{\xi\in[0,\tau]} \|\frac{q\nu}{\mathcal{ABC}(\nu)\Gamma(\nu)}\int_0^t(\tau-s)^{\nu-1}s^{q-1}\mathbb{V}(s,\mathcal{Z}(s))ds\Big| \\ &\leqslant \frac{q\nu}{\mathcal{ABC}(\nu)\Gamma(\nu)}\int_0^{\xi}(s)^{\nu-1}(1-s)^{r-1}|\mathbb{V}(s,\mathcal{Z}(s))|ds \leqslant \frac{q[\mathscr{X}_{\mathbb{V}}|\mathcal{Z}|+\mathscr{V}_{\mathbb{V}}\mathsf{T}^{\nu+q-1}]}{\mathcal{ABC}(\nu)\Gamma(\nu)}[\mathsf{B}(\nu,q)].\end{aligned} \tag{3.4}$$

Therefore, considering (3.4), the operator **H** is bounded. To demonstrate equi-continuity, suppose $t_1 > t_2 \in [0,\tau]$. We have

$$\begin{aligned}\big|\mathbf{H}(\mathcal{Z}(\mathbf{t_2}))-\mathbf{H}(\mathcal{Z}(\mathbf{t_1}))\big| &= \frac{q\nu}{\mathcal{ABC}(\nu)\Gamma(\nu)}\Big|\int_0^{t_2}(t_2-x)^{\nu-1}x^{q-1}\mathbb{V}(x,\mathcal{Z}(x))dx-\int_0^{t_1}(t_1-x)^{\nu-1}x^{q-1}\mathbb{V}(x,\mathcal{Z}(x))dx\Big|, \\ &\leqslant \frac{q[\mathscr{X}_{\mathbb{V}}|\mathcal{Z}|+\mathscr{V}_{\mathbb{V}}\mathsf{T}^{\nu+q-1}]\mathsf{B}(\nu,q)}{\mathcal{ABC}(\nu)\Gamma(\nu)}[t_2^{\nu}-t_1^{\nu}].\end{aligned}$$

As $t_2 \to t_1$, right hand side of (3.4) goes to zero. It is also possible to use the continuous operator G so

$$|\mathbf{H}\mathcal{Z}(\mathbf{t_2})-\mathbf{H}\mathcal{Z}(\mathbf{t_1})| \to \mathbf{0}, \text{ as } \mathbf{t_2}\to\mathbf{t_1}.$$

Thus, we have demonstrated that the operator **H** is both bounded and continuous, implying that it is both bounded and uniformly continuous. "Arzelà-Ascoli theorem" says that a closed, bounded, and equi-continuous subset of **G** will be compact. By analyzing (1.2) and (3.2), we can deduce that **H** is relatively compact and completely continuous. □

3.1. Uniqueness

Theorem 3.2. *In the case where* (J2) *can be assumed to be the global solution for the system* (3.2)*, it follows that the system* (1.2) *can be assumed to also possess a global solution if:*

$$\left[\frac{(1-\nu)t^{q-1}\mathbb{X}_{\mathbb{V}}}{\mathcal{ABC}(\nu)}+\frac{q[\mathbb{L}_{\mathbb{V}}\mathsf{T}^{\nu+q-1}]B(\nu,q)}{\mathcal{ABC}(\nu)\Gamma(\nu)}\right]<1.$$

Proof. Suppose the operator $\mathscr{T}:\mathcal{Z}\to\mathcal{Z}$ by

$$\begin{aligned}\mathscr{T}\mathcal{Z}(\xi) &= \mathcal{Z}_0(\xi)+\left[\mathbb{V}(\xi,\mathcal{Z}(\xi))-\mathbb{V}_0(\xi)\right]\frac{(1-\nu)\xi^{q-1}}{\mathcal{ABC}(\nu)} \\ &\quad+\frac{q\nu}{\mathcal{ABC}(\nu)\Gamma(\nu)}\int_0^{\xi}(\xi-x)^{\nu-1}\xi^{q-1}\mathbb{V}(x,\mathcal{Z}(x))dx,\ \xi\in[0,\tau].\end{aligned}$$

Let $\mathcal{Z},\bar{\mathcal{Z}}\in\mathcal{Z}$, then

$$+\frac{q\nu}{\mathcal{ABC}(\nu)\Gamma(\nu)}\max_{\xi\in[0,\tau]}\left|\int_0^{\xi}(\xi-x)^{\nu-1}\xi^{q-1}\mathbb{V}(x,\mathcal{Z}(x))dx-\int_0^{\xi}(\xi-x)^{\nu-1}\xi^{q-1}\mathbb{V}(x,\bar{\mathcal{Z}}(x))dx\right|\leqslant\Theta\|\mathcal{Z}-\bar{\mathcal{Z}}\|, \tag{3.5}$$

and

$$\Theta=\left[\frac{(1-\nu)\xi^{q-1}\mathbb{L}_{\mathbb{V}}}{\mathcal{ABC}(\nu)}+\frac{q[\mathbb{L}_{\mathbb{V}}\mathsf{T}^{\nu+q-1}]\mathsf{B}(\nu,q)\mathbb{L}_{\mathbb{V}}}{\mathcal{ABC}(\nu)\Gamma(\nu)}\right].$$

Based on (3.5), $\mathscr{T}$ is a contraction. Therefore, Eq. (3.2) has a unique solution. A unique solution exists for the system considered by (1.2). □

3.2. Ulam-Hyer stability

In this section, we determine if the proposed system (1.2) is stable. Let's change $(\Psi(\xi) \in C[0,T]$ a small amount and only check for stability, $0 = \Psi(0)$ as

- $|\Psi(\xi)| \leqslant \epsilon$ for $\epsilon > 0$;
- ${}^{\mathcal{ABC}}D_{\xi}^{(v,q)}\mathcal{Z}(\xi) = \mathbb{V}(\xi, \mathcal{Z}(\xi)) + \Psi(\xi)$.

Lemma 3.3. *The changed problem solution can be as*

$$ {}^{\mathcal{ABC}}D_{\xi}^{v,q}\mathcal{Z}(\xi) = \mathbb{V}(\xi, \mathcal{Z}(\xi)) + \Psi(\xi), \quad \mathcal{Z}(0) = \mathcal{Z}_0.$$

The given relation is satisfied the following

$$\begin{aligned}\left|\mathcal{Z}(\xi) - \left(\mathcal{Z}_0(\xi) + \left[\mathbb{V}(\xi, \mathcal{Z}(\xi)) - \Phi_0(\xi)\right]\frac{(1-v)}{\mathcal{ABC}(v)}\xi^{q-1}\right.\right.\\ \left.\left. + \frac{qv}{\mathcal{ABC}(v)\Gamma(v)}\int_0^{\xi}(\xi - x)^{v-1}x^{q-1}\mathbb{V}(x, \mathcal{Z}(x))dx\right)\right| \leqslant \frac{\Gamma(v)\xi^{q-1} + q\mathsf{T}^{v+q-1}}{\mathcal{ABC}(v)\Gamma(v)}B(v,q)\varepsilon = v_{v,q}\varepsilon.\end{aligned} \tag{3.6}$$

Theorem 3.4. *Based on the assumption* (C2)*, together with Eq.* (3.6)*, the solution of equation is UH stable, and therefore the analytical solution for the proposed system is UH stable if* $\Theta < 1$.

Proof. Assuming there is a unique solution to Eq. (3.2), and $\mathcal{Z} \in \mathcal{Z}$ is any solution of Eq. (3.2), then

$$\begin{aligned}&|\mathcal{Z}(\xi) - \bar{\mathcal{Z}}(\xi)|\\ &= \left|\mathcal{Z}(\xi) - \left(\mathcal{Z}_0(\xi) + \left[\mathbb{V}(\xi, \bar{\mathcal{Z}}(\xi)) - \mathbb{V}_0(\xi)\right]\frac{(1-v)}{\mathcal{ABC}(v)}\xi^{q-1} + \frac{qv}{\mathcal{ABC}(v)\Gamma(v)}\int_0^{\xi}(\xi - x)^{v-1}x^{q-1}\mathbb{V}(x, \bar{\mathcal{Z}}(x))dx\right)\right|\\ &\leqslant \left|\mathcal{Z}(\xi) - \left(\mathcal{Z}_0(\xi) + \left[\mathbb{V}(\xi, (\xi)) - \mathbb{V}_0(\xi)\right]\frac{(1-v)}{\mathcal{ABC}(v)}\xi^{q-1} + \frac{qv}{\mathcal{ABC}(v)\Gamma(v)}\int_0^{\xi}(\xi - x)^{v-1}x^{q-1}\mathbb{V}(x, (x))dx\right)\right|\\ &\quad + \left|\left(\mathcal{Z}_0(\xi) + \left[\mathbb{V}(\xi, (\xi)) - \mathbb{V}_0(\xi)\right]\frac{(1-v)}{\mathcal{ABC}(v)}\xi^{q-1} + \frac{qv}{\mathcal{ABC}(v)\Gamma(v)}\int_0^{\xi}(\xi - x)^{v-1}x^{q-1}\mathbb{V}(x, (x))dx\right)\right.\\ &\quad \left. - \left(\mathcal{Z}_0(\xi) + \left[(t, \bar{\mathcal{Z}}(\xi)) - \mathbb{V}_0(\xi)\right]\frac{(1-v)}{\mathcal{ABC}(v)}t^{q-1} + \frac{qv}{\mathcal{ABC}(v)\Gamma(v)}\int_0^{\xi}(\xi - x)^{v-1}x^{q-1}\mathbb{V}(x, \bar{\mathcal{Z}}(x))dx\right)\right|,\\ &\leqslant v_{v,q} + \frac{(1-v)\mathbb{L}_{\mathbb{V}}}{\mathcal{ABC}(v)}\xi^{q-1}\|\mathcal{Z} - \bar{\mathcal{Z}}\| + \frac{q\mathsf{T}^{v+q-1}\mathbb{L}_{\mathbb{V}}}{\mathcal{ABC}(v)\Gamma(v)}B(v,q)\|\mathcal{Z} - \bar{\mathcal{Z}}\| \leqslant v_{v,q} + \Theta\|\mathcal{Z} - \bar{\mathcal{Z}}\|.\end{aligned}$$

As a result of the above equation, we can write

$$\|\mathcal{Z} - \bar{\mathcal{Z}}\| \leqslant \frac{v_{v,q}}{1-\Theta}\left\|\mathcal{Z} - \bar{\mathcal{Z}}\right\|. \tag{3.7}$$

By using $\mathbb{V}_{\mathcal{Z}}(\varepsilon) = v_{v,q}\varepsilon, \mathbb{V}(0) = 0$, we concluded that the solution of (3.2) is UH stable from (3.7). There is a possibility that the proposed problem is Ulam-Hyers stable, as well as a possibility that it is generalized Ulam-Hyers stable, since the solution of the proposed problem is also Ulam-Hyers stable. □

4. Numerical scheme

In this section, we find the numerical solutions for the considered system (1.2) by using the $\mathcal{ABC}$ derivative based on the well-known fractal-fractional Adams-Bashforth (AB) technique. Using the fractal-fractional AB techniques described in [18], we obtain an approximate solution for the system (1.2). As a

result, (3.1) can be written as follows:

$$\begin{cases} {}^{\mathcal{ABC}}\mathrm{D}^{v}(\mathbb{S}(\xi)) = q\xi^{q-1}(\mathcal{M}_1(\mathbb{S}(\xi),\xi), \\ {}^{\mathcal{ABC}}\mathrm{D}^{v}(\mathbb{E}(\xi)) = q\xi^{q-1}(\mathcal{M}_2(\mathbb{E}(\xi),\xi), \\ {}^{\mathcal{ABC}}\mathrm{D}^{v}(\mathbb{I}(\xi)) = q\xi^{q-1}(\mathcal{M}_3(\mathbb{I}(\xi),\xi), \\ {}^{\mathcal{ABC}}\mathrm{D}^{v}(\mathbb{A}(\xi)) = q\xi^{q-1}(\mathcal{M}_4(\mathbb{A}(\xi),\xi), \\ {}^{\mathcal{ABC}}\mathrm{D}^{v}(\mathbb{R}(\xi)) = q\xi^{q-1}(\mathcal{M}_5(\mathbb{R}(\xi),\xi), \\ {}^{\mathcal{ABC}}\mathrm{D}^{v}(\mathbb{G}(\xi)) = q\xi^{q-1}(\mathcal{M}_6(\mathbb{G}(\xi),\xi), \end{cases}$$

where $(\mathcal{M}_k, k = 1,2,3,\ldots,6)$ is defined in equation (3.1). We can obtain the following results by applying the antiderivative of fractional order and fractal dimension to the first equation of (3.1) by using the $\mathcal{ABC}$ form as per the example below:

$$\mathbb{S}(\xi) - \mathbb{S}_{(0)} = \frac{(1-v)}{\mathcal{ABC}(v)}\xi^{q-1}\Big[(\mathcal{M}_1(\mathbb{S}(\xi),,\xi)\Big] + \frac{qv}{\mathcal{ABC}(v)\Gamma(v)}\int_0^{\xi}(\xi-x)^{v-1}x^{,-1}(\mathcal{M}_1(\mathbb{S}(x),x)\,dx.$$

Set $\xi = \xi_{b+1}$ for $k = 0,1,2,\ldots,$

$$\begin{aligned} &\mathbb{S}(\xi_{b+1}) - \mathbb{S}_{(0)} \\ &= \frac{(1-v)}{\mathcal{ABC}(v)}(\xi_{b+1}^{q-1})\Big[(\mathcal{M}_1(\mathbb{S}(\xi_b),t_b)\Big] + \frac{qv}{\mathcal{ABC}(v)\Gamma(v)}\int_0^{\xi_{b+1}}(\xi_{b+1}-x)^{v-1}x^{q-1}(\mathcal{M}_1(\mathbb{S}(x),(x))\,dx, \\ &= \frac{(1-v)}{\mathcal{ABC}(v)}(\xi_{b+1}^{q-1})\Big[(\mathcal{M}_1(\mathbb{S}(\xi_b),\xi_b)\Big] + \frac{qv}{\mathcal{ABC}(v)\Gamma(v)}\sum_{r=0}^{c}\int_r^{t_{r+1}}(\xi_{b+1}-x)^{v-1}x^{q-1}(\mathcal{M}_1(\mathbb{S}(x),x)\,dx. \end{aligned}$$

The approximation of the function be $\mathcal{M}_1$ on the interval $[\xi_r,\xi_{r+1}]$ is achieved through the interpolation polynomial as follows

$$\mathcal{M}_1 \cong \frac{\mathcal{M}_1}{\Delta}(\xi-\xi_{r-1}) - \frac{\mathbf{R}_1}{\Delta}(\xi-\xi_r),$$

which implies that

$$\begin{aligned} \mathbb{S}(\xi_{b+1}) &= \mathbb{S}_{(0)} + \frac{(1-v)}{\mathcal{ABC}(v)}(\xi_{b+1}^{q-1})\Big[\mathcal{M}_1(\mathbb{S}(\xi_b),\xi_b)\Big] + \frac{qv}{\mathcal{ABC}(v)\Gamma(v)}\sum_{r=0}^{c}\Bigg(\frac{\mathcal{M}_1(\mathbb{S}(\xi_b),\xi_b)}{\Delta} \\ &\quad\times\int_r^{\xi_{r+1}}(\xi-\xi_{r-1})(\xi_{r+1}-\xi)^{v-1}\xi_r^{q-1}d\xi - \frac{\mathcal{M}_1(\mathbb{S}(\xi_b),\xi_b)}{\Delta}\int_r^{\xi_{r+1}}(\xi-\xi_r)(\xi_{b+1}-\xi)^{v-1}\xi_r^{q-1}d\xi\Bigg), \\ \mathbb{S}(\xi_{b+1}) &= \mathbb{S}_{(}0) + \frac{(1-v)}{\mathcal{ABC}(v)}(\xi_{b+1}^{q-1})\Big[\mathcal{M}_1(\mathbb{S}(\xi_b),\xi_b)\Big] \\ &\quad+ \frac{qv}{\mathcal{ABC}(v)\Gamma(v)}\sum_{r=0}^{c}\Bigg(\frac{\xi_r^{q-1}\mathcal{M}_1(\mathbb{S}(\xi_r),\xi_r)}{\Delta}I_{r-1,v} - \frac{\xi_{r-1}^{q-1}\mathcal{M}_1(\mathbb{S}(\xi_{r-1}),\xi_{r-1})}{\Delta}I_{r,v}\Bigg). \end{aligned} \tag{4.1}$$

Calculating $I_{r-1,v}$ and $I_{r,v}$ we get

$$\begin{aligned} I_{r-1,v} &= \int_r^{\xi_{r+1}}(\xi-\xi_{r-1})(\xi_{b+1}-\xi)^{v-1}d\xi \\ &= -\frac{1}{v}\Big[(\xi_{r+1}-\xi_{r-1})(\xi_{b+1}-\xi_{r+1})^{\sigma} - (\xi_r-\xi_{r-1})(\xi_{b+1}-\xi_r)^{\sigma}\Big] \\ &\quad - \frac{1}{v(v-1)}\Big[(\xi_{b+1}-\xi_{r+1})^{v+1} - (\xi_{b+1}-\xi_r)^{v+1}\Big], \end{aligned}$$

and

$$I_{r,v} = \int_r^{\xi_{r+1}}(\xi-\xi_r)(\xi_{b+1}-\xi)^{v-1}d\xi,$$

$$= -\frac{1}{v}\left[(\xi_{r+1}-\xi_r)(\xi_{b+1}-\xi_{r+1})^v\right] - \frac{1}{v(v-1)}\left[(\xi_{b+1}-t_{r+1})^{v+1} - (\xi_{b+1}-\xi_r)^{\sigma+1}\right],$$

putting $\xi_r = r\Delta$, we get

$$\begin{aligned}
I_{r-1,v} &= -\frac{\Delta^{v+1}}{v}\left[(r+1-(r-1))(b+1-(r+1))^v - (r-(r-1))(b+1-r^v)\right] \\
&\quad - \frac{\Delta^{v+1}}{v(v-1)}\left[(b+1-(r+1))^{v+1} - (b+1-r)^{v+1}\right] \\
&= \frac{\Delta^{v+1}}{v(v-1)}\left[-2(v+1)(b-r)^v + (v+1)(b+1-r)^v - (b-r)^{v+1} + (b+1-r)^{v+1}\right] \\
&= \frac{\Delta^{v+1}}{v(v-1)}\left[(b-r)^v(-2(v+1)-(b-r)) + (b+1-r)^v(v+1+b+1-r)\right] \\
&= \frac{\Delta^{v+1}}{v(v-1)}\left[(b+1-r)^v(b-r+2+v) - (b-r)^v(b-r+2+2v)\right],
\end{aligned} \tag{4.2}$$

and

$$\begin{aligned}
I_{r,v} &= -\frac{\Delta^{v+1}}{v}\left[(r+1-r)(b+1-(r+1))^v\right] - \frac{\Delta^{v+1}}{v(v-1)}\left[(b+1-(r+1))^{v+1} - (b+1-r)^{v+1}\right] \\
&= \frac{\Delta^{v+1}}{v(v-1)}\left[-(v+1)(b-r)^v - (b-r)^{v+1} + (b+1-r)^{v+1}\right] \\
&= \frac{\Delta^{v+1}}{v(v-1)}\left[(b-r)^v(-(r+1)-(b-r)) + (b+1-r)^{v+1}\right] \\
&= \frac{\Delta^{v+1}}{v(v-1)}\left[(b+1-r)^{v+1} - (b-r)^v(b-r+1+v)\right].
\end{aligned} \tag{4.3}$$

After substituting equation (4.2) and equation (4.3) into equation (4.1), we obtain

$$\begin{aligned}
S(\xi_{b+1}) &= S(0) + \frac{(1-v)}{\mathcal{ABC}(v)}(\xi_{b+1}^{q-1})\left[\mathcal{M}_1\big(S(\xi_b),\xi_b\big)\right] + \frac{qv}{\mathcal{ABC}(v)\Gamma(v)}\sum_{r=0}^{b}\Bigg(\frac{\xi_r^{q-1}\mathcal{M}_1\big(S(\xi_r),\xi_r\big)}{\Delta} \\
&\quad \times\left[\frac{\Delta^{v+1}}{v(v-1)}\left[(b+1-r)^v(b-r+2+v) - (b-r)^v(b-r+2+2v)\right]\right] \\
&\quad - \frac{\xi_{r-1}^{q-1}\mathcal{M}_1\big(S(\xi_{r-1}),t_{r-1}\big)}{\Delta}\left[\frac{\Delta^{v+1}}{v(v-1)}\left[(b+1-r)^{v+1} - (b-r)^v(b-r+1+v)\right]\right]\Bigg).
\end{aligned}$$

Similarly, we can apply the same numerical scheme to the remaining classes $\mathbb{E}, \mathbb{I}, \mathbb{A}, \mathbb{R}$, and $\mathbb{G}$ as

$$\begin{aligned}
\mathbb{E}(\xi_{b+1}) &= \mathbb{E}(0) + \frac{(1-v)}{\mathcal{ABC}(v)}(\xi_{b+1}^{q-1})\left[\mathcal{M}_2\big(\mathbb{E}(\xi_b),\xi_b\big)\right] + \frac{qv}{\mathcal{ABC}(v)\Gamma(v)}\sum_{r=0}^{b}\Bigg(\frac{\xi_r^{q-1}\mathcal{M}_2\big(\mathbb{E}(\xi_r),\xi_r\big)}{\Delta} \\
&\quad \times\left[\frac{\Delta^{v+1}}{v(v-1)}\left[(b+1-r)^v(b-r+2+v) - (b-r)^v(b-r+2+2v)\right]\right] \\
&\quad - \frac{\xi_{r-1}^{q-1}\mathcal{M}_2\big(\mathbb{E}(\xi_{r-1}),\xi_{r-1}\big)}{\Delta}\left[\frac{\Delta^{v+1}}{v(v-1)}\left[(b+1-r)^{v+1} - (b-r)^v(b-r+1+v)\right]\right]\Bigg), \\
\mathbb{I}(\xi_{b+1}) &= \mathbb{I}(0) + \frac{(1-v)}{\mathcal{ABC}(v)}(\xi_{b+1}^{q-1})\left[\mathcal{M}_3\big(\mathbb{I}(\xi_b),\xi_b\big)\right] + \frac{qv}{\mathcal{ABC}(v)\Gamma(v)}\sum_{r=0}^{b}\Bigg(\frac{\xi_r^{q-1}\mathcal{M}_3\big(\mathbb{I}(\xi_r),\xi_r\big)}{\Delta} \\
&\quad \times\left[\frac{\Delta^{v+1}}{v(v-1)}\left[(b+1-r)^v(b-r+2+v) - (b-r)^v(b-r+2+2v)\right]\right]
\end{aligned}$$

$$
\begin{aligned}
&- \frac{\xi_{r-1}^{q-1}\mathcal{M}_3\big(\mathbb{I}(\xi_{r-1}),\xi_{r-1}\big)}{\Delta}\left[\frac{\Delta^{v+1}}{v(v-1)}\left[(b+1-r)^{v+1}-(b-r)^{v}(b-r+1+v)\right]\right]\Bigg),\\
\mathbb{A}(\xi_{b+1}) &= \mathbb{A}(0)+\frac{(1-v)}{\mathcal{ABC}(v)}(\xi_{b+1}^{q-1})\left[\mathcal{M}_4\big(\mathbb{A}(\xi_b),\xi_b\big)\right]+\frac{qv}{\mathcal{ABC}(v)\Gamma(v)}\sum_{r=0}^{b}\Bigg(\frac{\xi_r^{q-1}\mathcal{M}_4\big(\mathbb{A}(t_r),\xi_r\big)}{\Delta}\\
&\times\left[\frac{\Delta^{v+1}}{v(v-1)}\left[(b+1-r)^{v}(b-r+2+v)-(b-r)^{v}(b-r+2+2v)\right]\right]\\
&- \frac{\xi_{r-1}^{q-1}\mathcal{M}_4\big(\mathbb{A}(\xi_{r-1}),\xi_{r-1}\big)}{\Delta}\left[\frac{\Delta^{v+1}}{v(v-1)}\left[(b+1-r)^{v+1}-(b-r)^{v}(b-r+1+v)\right]\right]\Bigg),\\
(\mathbb{R}(t_{b+1}) &= (\mathbb{R}(0)+\frac{(1-v)}{\mathcal{ABC}(v)}(\xi_{b+1}^{q-1})\left[\mathcal{M}_5\big(\mathbb{R}(\xi_b),\xi_b\big)\right]+\frac{qv}{\mathcal{ABC}(v)\Gamma(v)}\sum_{r=0}^{b}\Bigg(\frac{\xi_r^{q-1}\mathcal{M}_5\big(\mathbb{R}(\xi_r),\xi_r\big)}{\Delta}\\
&\times\left[\frac{\Delta^{v+1}}{v(v-1)}\left[(b+1-r)^{v}(b-r+2+v)-(b-r)^{v}(b-r+2+2v)\right]\right]\\
&- \frac{\xi_{r-1}^{q-1}\mathcal{M}_5\big(\mathbb{R}(\xi_{r-1}),\xi_{r-1}\big)}{\Delta}\left[\frac{\Delta^{v+1}}{v(v-1)}\left[(b+1-r)^{v+1}-(b-r)^{v}(b-r+1+v)\right]\right]\Bigg),\\
(\mathbb{G}(\xi_{b+1}) &= (\mathbb{G}(0)+\frac{(1-v)}{\mathcal{ABC}(v)}(\xi_{b+1}^{q-1})\left[\mathcal{M}_6\big(\mathbb{G}(\xi_b),\xi_b\big)\right]+\frac{qv}{\mathcal{ABC}(v)\Gamma(v)}\sum_{r=0}^{b}\Bigg(\frac{\xi_r^{q-1}\mathcal{M}_6\big(\mathbb{G}(\xi_r),\xi_r\big)}{\Delta}\\
&\times\left[\frac{\Delta^{v+1}}{v(v-1)}\left[(b+1-r)^{v}(b-r+2+v)-(b-r)^{v}(b-r+2+2v)\right]\right]\\
&- \frac{\xi_{r-1}^{q-1}\mathcal{M}_6\big(\mathbb{G}(\xi_{r-1}),\xi_{r-1}\big)}{\Delta}\left[\frac{\Delta^{v+1}}{v(v-1)}\left[(b+1-r)^{v+1}-(b-r)^{v}(b-r+1+v)\right]\right]\Bigg).
\end{aligned}
$$

5. Simulations results

The considered system (1.2) values have been compiled in the table below and provided in a tabular format. This section of the paper introduces numerical simulations of model system (1.2) utilizing the MATLAB 21 solver to carry out numerical simulations. As a first step towards understanding the specific behavior of the model, we have chosen arbitrary initial conditions for the model: $\mathbb{S}=4000, \mathbb{E}=3000, \mathbb{I}=2000, \mathbb{A}=1000, \mathbb{R}=800$, and $\mathbb{G}=50000$. Various graphical representations, which were discussed, support the analytical results. For illustrative purposes, we used values gleaned from the literature and made some assumptions given the unavailability of numerous parameters. Simulations were performed using parameter values from Table 2.

Table 2: The values of the model's parameters (2).

Parameter	Value per day	Source	Parameter	Value per day	Source
Λ	0.036-0.06	[26, 40]	ρ	0.0001	Supposed
β_1	0.00035	[26, 37]	β_2	0.00034	Supposed
β_3	0.00034	[26]	κ	0.0001	Supposed
μ	0.00004215	[37]	α	0.001	Supposed
ν	0.0025	Supposed	γ	0.5-0.04	[26]
η	0.1	Supposed	ψ	0.00001	Supposed
p	0.0714	[40]	δ	0.001	Supposed
ϵ	0.25	[26]	d	0.0025	Supposed
τ	0.03	[26]	σ	0.01	Supposed
χ	0.5	Supposed			

We have applied a deep neural network (DNN) method for the model under consideration with the $\mathcal{ABC}$ fractal-fractional operator in this part. We have selected three hidden layers, with 10, 100, and 10 neurons in each hidden layer, in order to proceed further. To get a better set of weight with less residual errors, the Levenberg-Marquardt technique is applied, with the epochs number being taken as 1000. The DNN datasets are analyzed using the fractional Adams-Bashforth method. Plots of the suggested model show the approximate solutions that we obtained by using the DNN to train the data set.

Figure 1a represent all data for $\mathbb{S}$ class and the output is obtained by DNN. In this Figure the regression coefficient is approximately 1, the mean square 0.009276 and root mean square errors 0.096316 obtained for this class. The histogram represented mean and variance errors and the errors are 0.0018153 and 0.096307 which show the accuracy of the proposed technique. Figure 1b represent train data for $\mathbb{S}$ class and the output is obtained with the same method. In the figure the regression coefficient is approximately 1, the mean square 0.0092481 and root mean square errors 0.096167 obtained for this class. Histogram represented mean and variance errors and the errors are $3.2109e-05$ and 0.096178 which show the accuracy of the proposed technique. Figure 1c represent test data for $\mathbb{S}$ class and the output is obtained with the same method, the regression coefficient is approximately 1, the mean square 0.0075467 and root mean square errors 0.086872 obtained for this class. Histogram represented mean and variance errors and the errors are 0.0041069 and 0.086823 which show the accuracy of the proposed technique. Similarly, Figure 1d represent validation data for $\mathbb{S}$ class and the output is obtained with the same method, the regression coefficient is approximately 1, the mean square 0.011141 and root mean square errors 0.10555 obtained for this class. Histogram represented mean and variance errors and the errors are 0.0078472 and 0.10532 which show the accuracy of the proposed technique. Figure 1e shows the dynamics of the first class comparison with DNN.

Figure 2a represent all data for $\mathbb{E}$ class and the output is obtained by DNN. In this figure the regression coefficient is approximately 1, the mean square 34.89 and root mean square errors 5.9068 obtained for this class. The histogram represented mean and variance errors and the errors are 0.059959 and 5.907 which show the accuracy of the proposed technique. Figure 2b represent train data for $\mathbb{E}$ class and the output is obtained with the same method. In the figure the regression coefficient is approximately 1, the mean square 35.4893 and root mean square errors 5.9573 obtained for this class. Histogram represented mean and variance errors and the errors are 0.0014066 and 5.958 which show the accuracy of the proposed technique. Figure 2c represent test data for $\mathbb{E}$ class and the output is obtained with the same method, the regression coefficient is approximately 1, the mean square 35.8788 and root mean square errors 5.9899 obtained for this class. Histogram represented mean and variance errors and the errors are 0.19816 and 5.9899 which show the accuracy of the proposed technique. Similarly, Figure 2d represent validation data for $\mathbb{E}$ class and the output is obtained with DNN method, the regression coefficient is approximately 1, the mean square 31.1036 and root mean square errors 5.5771 obtained for this class. Histogram represented mean and variance errors and the errors are 0.19506 and 5.5768 which show the accuracy of the proposed technique. Figure 2e shows the dynamics of the first class comparison with DNN.

Figure 3a represent all data for $\mathbb{I}$ class and the output is obtained by DNN. In this figure the regression coefficient is approximately 1, the mean square 2.0877 and root mean square errors 1.4449 obtained for this class. The histogram represented mean and variance errors and the errors are 0.005032 and 1.445 which show the accuracy of the proposed technique. Figure 3b represent train data for $\mathbb{I}$ class and the output is obtained with the DNN method. In the figure, the regression coefficient is approximately 1, the mean square 1.9441 and root mean square errors 1.3943 obtained for this class. Histogram represented mean and variance errors and the errors are 0.00426 and 1.3945 which show the accuracy of the proposed technique. Figure 3c shows test data for $\mathbb{I}$ class and the output is obtained with the same method, the regression coefficient is approximately 1, the mean square 2.6836 and root mean square errors 1.6382 obtained for this class. Histogram represented mean and variance errors and the errors are 0.045142 and 1.6385 which show the accuracy of the proposed technique. Similarly, Figure 3d represent validation data for $\mathbb{I}$ class and the output is obtained with the same method, the regression coefficient is approximately 1, the mean square 2.1626 and root mean square errors 1.4706 obtained for this class. Histogram represented mean

and variance errors and the errors are -0.031474 and 1.4711 which show the accuracy of the proposed technique. Figure 3e shows the dynamics of the first class comparison with DNN.

Figure 4a represent all data for $\mathbb{A}$ class and the output is obtained by DNN. In this figure, the regression coefficient is approximately 1, the mean square $1.8809e-07$ and root mean square errors 0.0004337 obtained for this class. The histogram represented mean and variance errors and the errors are $5.3369e-06$ and 0.0004337 which show the accuracy of the proposed technique. Figure 4b represent train data set for $\mathbb{A}$ class and the output is obtained with the same method. In the figure, the regression coefficient is approximately 1, the mean square $1.7478e-07$ and root mean square errors 0.00041807 obtained for this class. Histogram represented mean and variance errors and the errors are $3.5416e-07$ and 0.00041812 which show the accuracy of the proposed technique. Figure 4c shows test data for $\mathbb{A}$ class and the output is obtained with the same method, the regression coefficient is approximately 1, the mean square $2.6544e-07$ and root mean square errors 0.00051521 obtained for this class. Histogram represented mean and variance errors and the errors are $1.9167e-05$ and 0.00051514 which show the accuracy of the proposed technique. Similarly, Figure 4d represent validation data for $\mathbb{A}$ class and the output is obtained with the same method, the regression coefficient is approximately 1, the mean square $1.7289e-07$ and root mean square errors 0.0004158 obtained for this class. Histogram represented mean and variance errors and the errors are $1.4765e-05$ and 0.00041577 which show the accuracy of the proposed technique. Figure 4e shows the dynamics of the first class comparison with DNN.

All data for $\mathbb{R}$ class are represented in Figure 5a, and the output is obtained by DNN. In this figure the regression coefficient is approximately 1, the mean square 16.056 and root mean square errors 4.007 obtained for this class. The histogram represented mean and variance errors and the errors are -0.04620 and 4.0071 which show the accuracy of the proposed technique. Figure 5b represent train data for $\mathbb{R}$ class and the output is obtained with the same method. In the figure, the regression coefficient is approximately 1, the mean square 15.1696 and root mean square errors 3.8948 obtained for this class. Histogram represented mean and variance errors and the errors are -0.0037725 and 3.8953 which show the accuracy of the proposed technique. Figure 5c shows test data for $\mathbb{R}$ class and the output is obtained with the same method, the regression coefficient is approximately 1, the mean square 20.15 and root mean square errors 4.4889 obtained for this class. Histogram represented mean and variance errors and the errors are 0.0025456 and 4.4914 which show the accuracy of the proposed technique. Similarly, validation data for $\mathbb{R}$ class is represented in Figure 5d and the output is obtained with the same method, the regression coefficient is approximately 1, the mean square 16.0996 and root mean square errors 4.0124 obtained for this class. Histogram represented mean and variance errors and the errors are -0.29299 and 4.0039 which show the accuracy of the proposed technique. Figure 5e shows the dynamics of the first class comparison with DNN.

Figure 6a shows all data for $\mathbb{G}$ class and the output is obtained by DNN. In this figure the regression coefficient is approximately 1, the mean square 0.94881 and root mean square errors 0.97407 obtained for this class. The histogram represented mean and variance errors and the errors are 0.0090399 and 0.97411 which show the accuracy of the proposed technique. Figure 6b represent train data for $\mathbb{G}$ class and the output is obtained with the same method. In the figure, the regression coefficient is approximately 1, the mean square 0.92049 and root mean square errors 0.95942 obtained for this class. Histogram represented mean and variance errors and the errors are -0.0023987 and 0.95953 which show the accuracy of the proposed technique. Figure 6c represent test data for $\mathbb{G}$ class and the output is obtained with the same method, the regression coefficient is approximately 1, the mean square 1.0774 and root mean square errors 1.038 obtained for this class. Histogram represented mean and variance errors and the errors are -0.0048193 and 1.0386 which show the accuracy of the proposed technique. Similarly, Figure 6d shows validation data for $\mathbb{G}$ class and the output is obtained with the same method, the regression coefficient is approximately 1, the mean square 0.95238 and root mean square errors 0.9759 obtained for this class. Histogram represented mean and variance errors and the errors are 0.076292 and 0.97345 which show the accuracy of the proposed technique. Figure 6e, show the dynamics of the first class comparison with DNN.

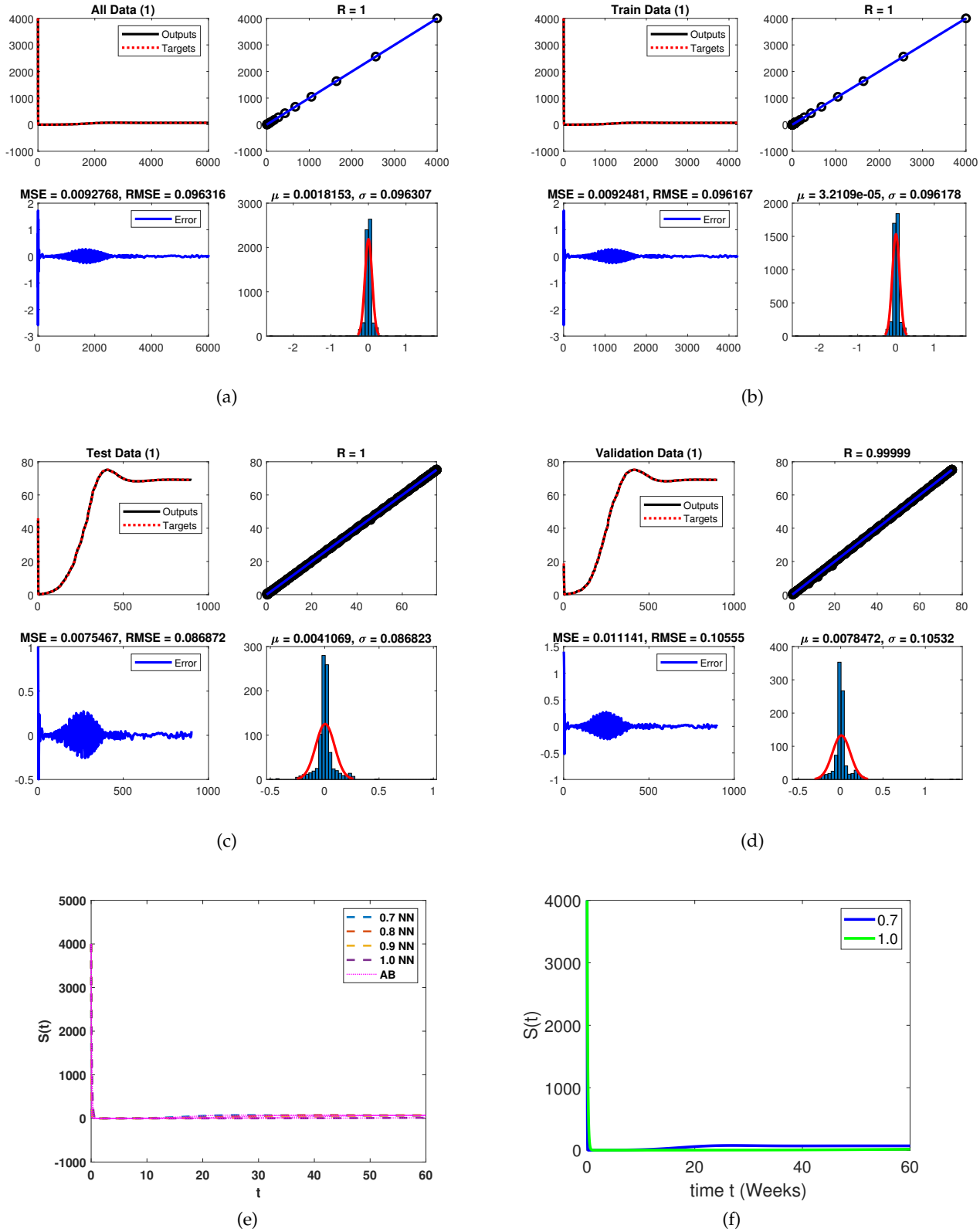

Figure 1: Dynamics of $S(t)$ with deep neural network (a) all data, (b) train data; (c) test data; (d) validation; (e) comparison of AB with NN; (f) comparison of fractional and integer order.

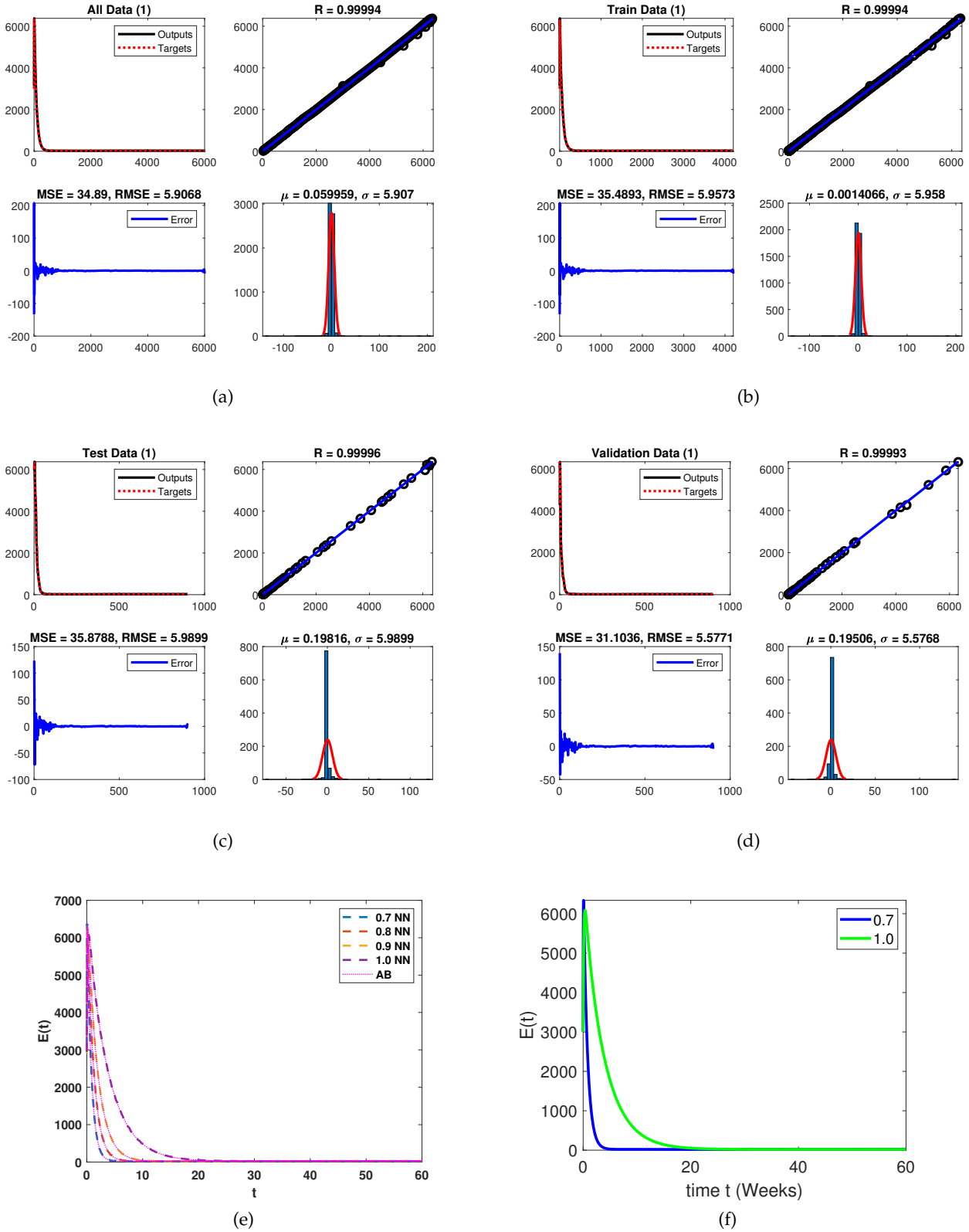

Figure 2: Dynamics of $E(t)$ with deep neural network (a) all data; (b) train data; (c) test data; (d) validation; (e) comparison of AB with NN; (f) comparison of fractional and integer order.

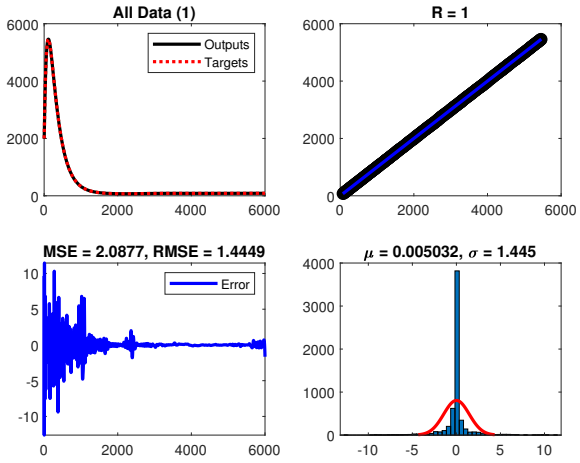

(a)

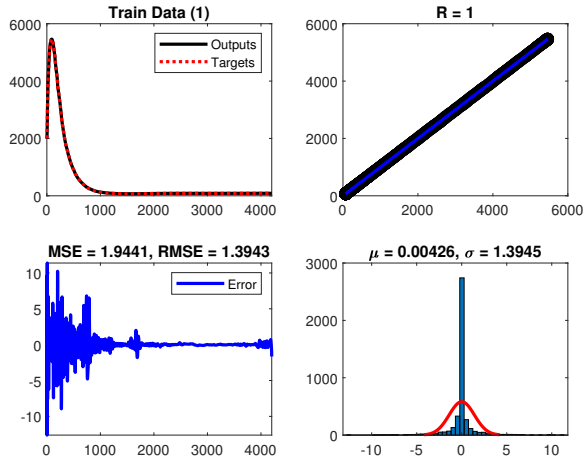

(b)

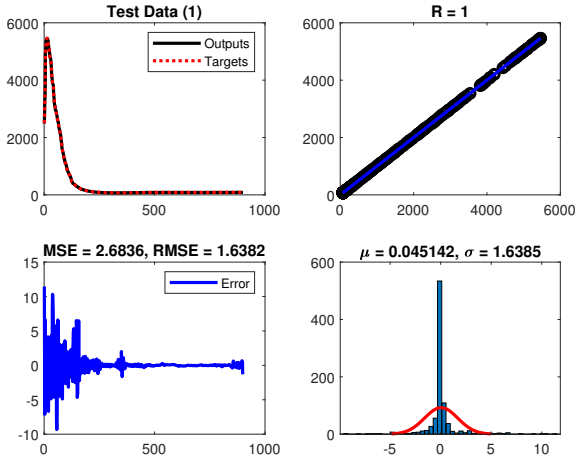

(c)

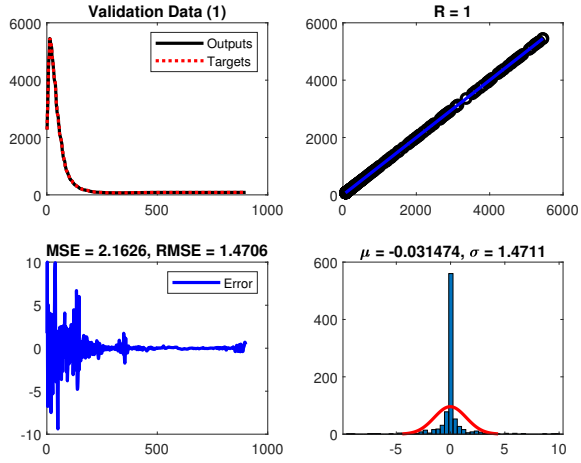

(d)

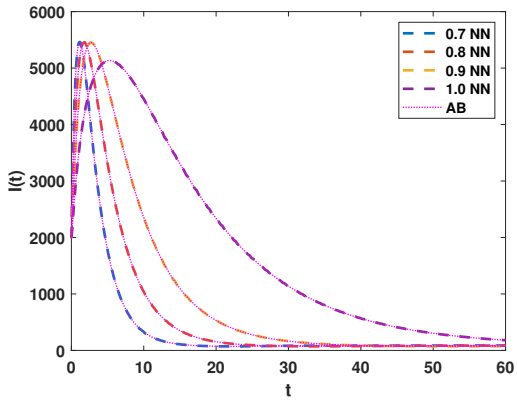

(e)

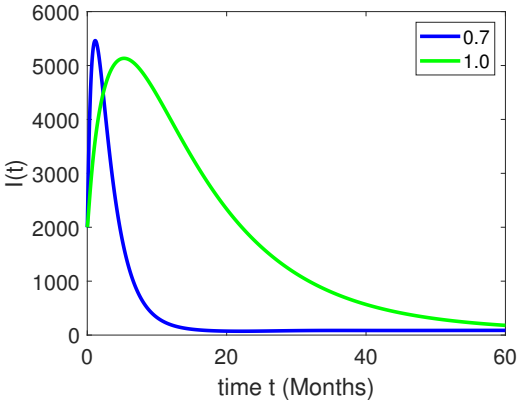

(f)

Figure 3: Dynamics of I(t) with deep neural network (a) all data; (b) train data; (c) test data; (d) validation; (e) comparison of AB with NN; (f) comparison of fractional and integer order.

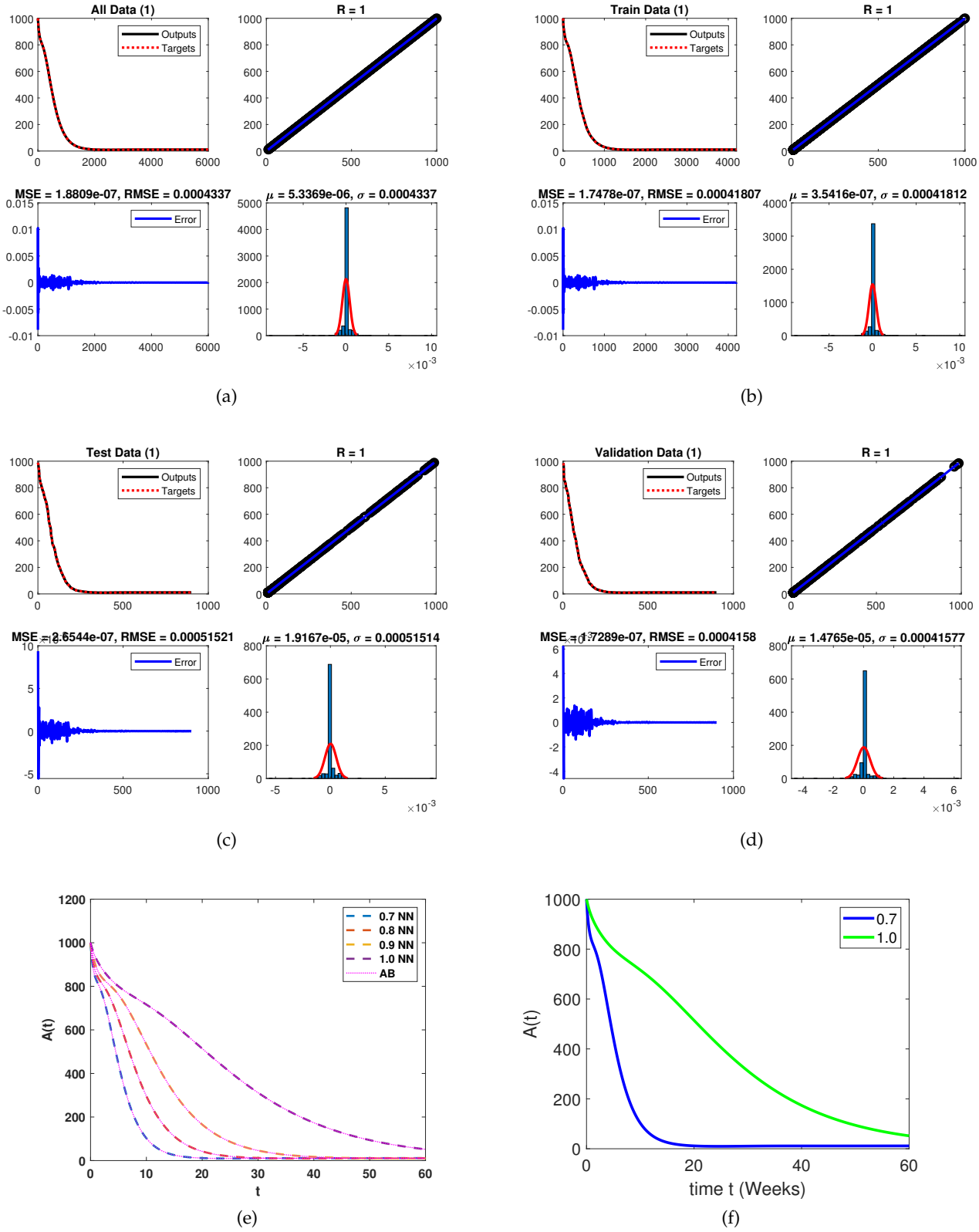

Figure 4: Dynamics of $A(t)$ with deep neural network (a) all data; (b) train data; (c) test data; (d) validation; (e) comparison of AB with NN; (f) comparison of fractional and integer order.

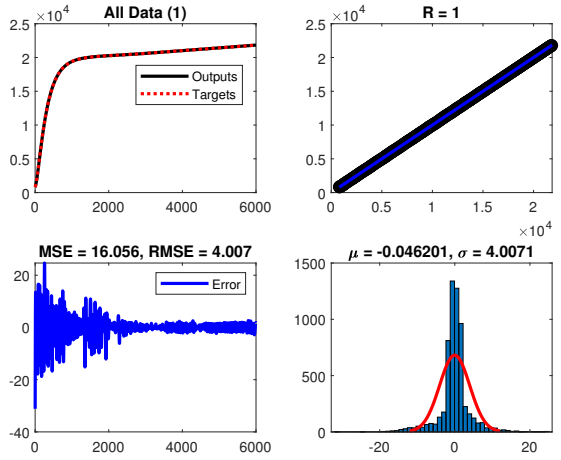

(a)

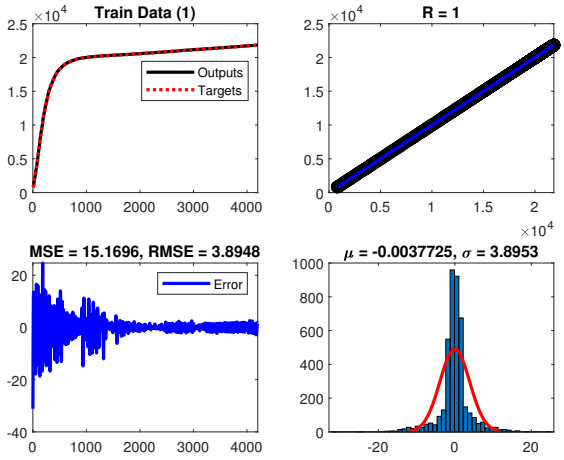

(b)

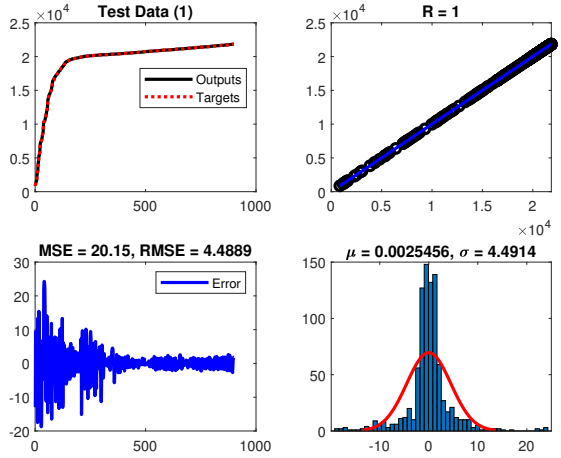

(c)

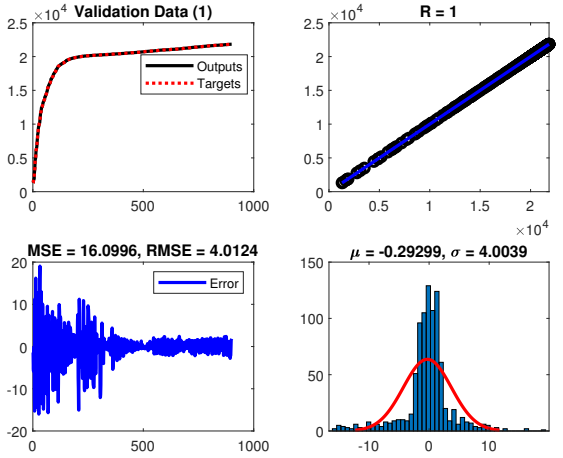

(d)

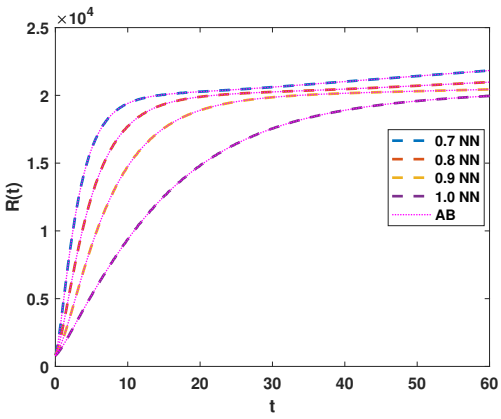

(e)

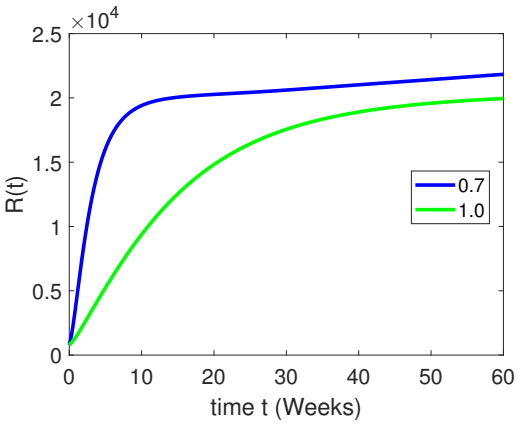

(f)

Figure 5: Dynamics of R(t) with deep neural network (a) all data; (b) train data; (c) test data; (d) validation; (e) comparison of AB with NN; (f) comparison of fractional and integer order.

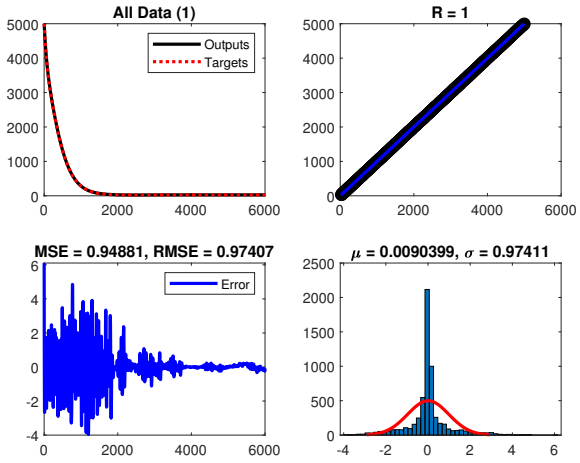

(a)

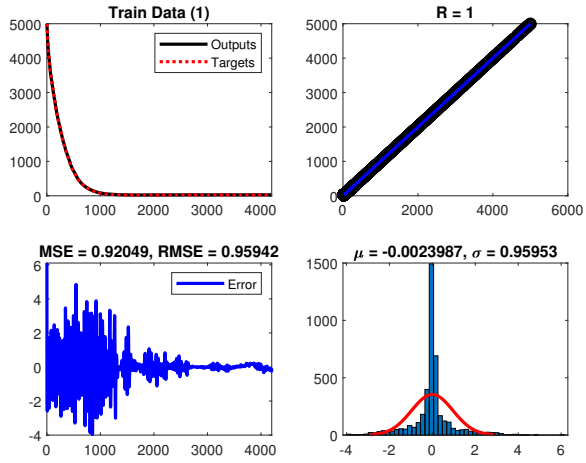

(b)

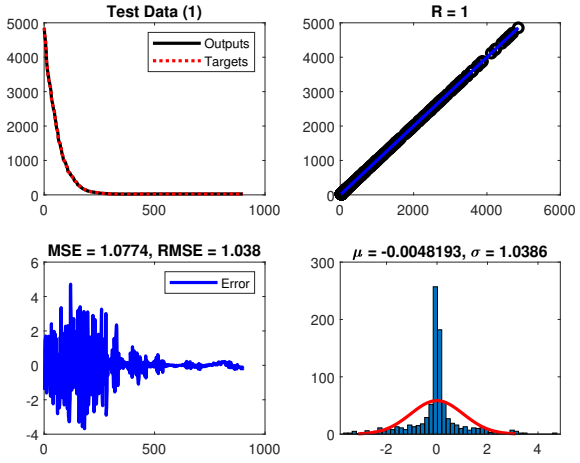

(c)

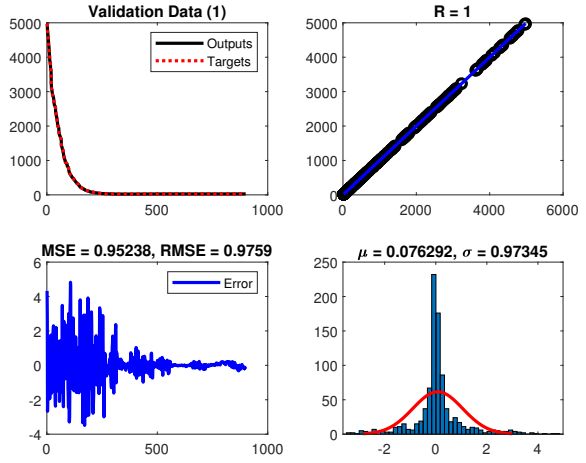

(d)

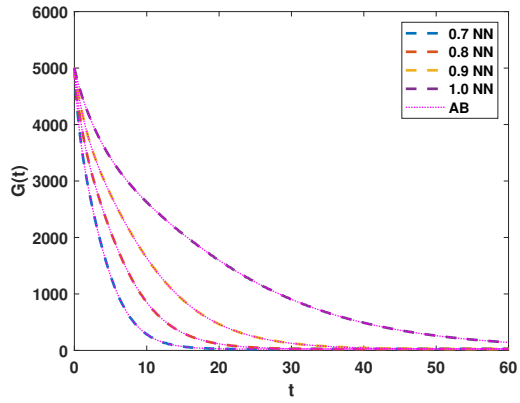

(e)

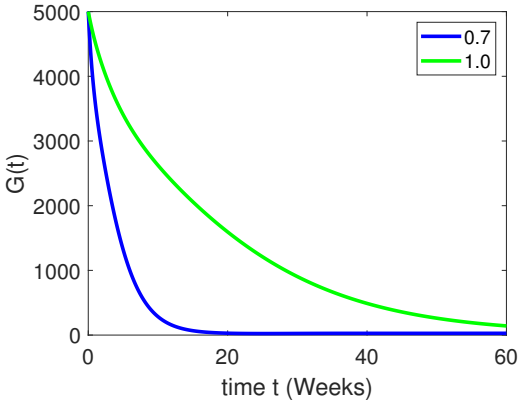

(f)

Figure 6: Dynamics of $R(t)$ with deep neural network (a) all data; (b) train data; (c) test data; (d) validation; (e) comparison of AB with NN; (f) comparison of fractional and integer order.

6. Concluding remark

In this study, a deterministic mathematical model has been developed and analyzed to understand the transmission dynamics of Giardiasis. Both direct and indirect transmission are considered in the model, which consists of six compartments: susceptible humans, exposed humans, infectious humans, recovered humans, and Giardia populations. Several interventions may be included with carriers present in the system of ordinary differential equations. Several strategies are incorporated into the model, including sanitation, treatment, and screening. The aim of this paper is to investigate the dynamics of a fractal-fractional modified nonlinear SEIR-type system with non-integer order and fractal dimension under the influence of the $\mathcal{ABC}$ derivative of a nonlinear SEIR system. Giardia population infection is being investigated to control and stabilize it. Theorems of nonlinear functional analysis are used in the qualitative analysis. For different fractional orders and fractal dimensions, Adams-Bashforth simulations demonstrate the dynamical behavior of each compartment. Each compartment is represented graphically by a density that lies between two integers. Low fractional orders and fractal dimensions require shorter memory times for stability and convergence. As a result of our analysis of the model parameters, it appears that hygiene, screening, and treatment control strategies have a negative value, indicating that they reduce the risk of disease transmission in communities as a whole. Over time, simulations suggest that the number of infectious individuals decreases rapidly as control interventions increase. According to mathematical simulations, combining all three interventions (treatment, screening, and sanitation) reduces disease prevalence in the population by a significant amount. The study notes, however, that these interventions play an essential role in increasing illness awareness, even though the model presented does not constitute an exhaustive model, and its assumptions can be adjusted accordingly. A cost-effectiveness approach to control measures may also be accommodated by adjusting assumptions. Giardiasis cases in communities can be reduced by a comprehensive approach to prevention, emphasizing the importance of public health education and intervention.

Acknowledgment

The authors extend their appreciation to Prince Sattam bin Abdulaziz University for funding this research work through the project number (PSAU/2024/01/99517).

References

[1] T. Abdeljawad, D. Baleanu, *Discrete fractional differences with nonsingular discrete Mittag-Leffler kernels*, Adv. Difference Equ., **2016** (2016), 18 pages. 2.3
[2] N. Ali, R. Khan, *Existence of positive solution to a class of fractional differential equations with three point boundary conditions*, Math. Sci. Lett., **5** (2016), 291–296. 1
[3] B. Ahmad, S. Sivasundaram, *On four-point nonlocal boundary value problems of nonlinear integro-differential equations of fractional order*, Appl. Math. Comput., **217** (2010), 480–487. 1
[4] A. Atangana, *Fractal-fractional differentiation and integration: connecting fractal calculus and fractional calculus to predict complex system*, Chaos solitons fractals, **102** (2017), 396–406. 1, 2.1, 2.2
[5] A. Atangana, *Modelling the spread of COVID-19 with new fractal-fractional operators: can the lockdown save mankind before vaccination?*, Chaos Solitons Fractals, **136** (2020), 38 pages. 1
[6] A. Atangana, S. İğret Araz, *Mathematical model of COVID-19 spread in Turkey and South Africa: theory, methods, and applications*, Adv. Difference Equ., **2020** (2020), 89 pages 1
[7] İ. Avcı, H. Lort, B. E. Tatlıcıoğlu, *Numerical investigation and deep learning approach for fractal-fractional order dynamics of Hopfield neural network model*, Chaos Solitons Fractals, **177** (2023), 14 pages. 1
[8] Z. Bai, *On positive solutions of a nonlocal fractional boundary value problem*, Nonlinear Anal., **72** (2010), 916–924. 1
[9] S. R. Birkeland, S. P. Preheim, B. J. Davids, M. J. Cipriano, D. Palm, D. S. Reiner, S. G. Svärd, F. D. Gillin, A. G. McArthur, *Transcriptome analyses of the giardia lamblia life cycle*, Mol. Biochem. Parasitol., **174** (2010), 62–65. 1
[10] R. T. Chen, Y. Rubanova, J. Bettencourt, D. K. Duvenaud, *Neural ordinary differential equations*, Adv. Neural Inf. Process. Syst., **31** (2018). 1
[11] M. Di Giovanni, D. Sondak, P. Protopapas, M. Brambilla, *Finding multiple solutions of odes with neural networks*, In: Combining Artificial Intelligence and Machine Learning with Physical Sciences 2020, CEUR-WS, **2587** (2020), 1–7. 1

[12] S. Etemad, A. Shikongo, K. M. Owolabi, B. Tellab, İ. Avcı, S. Rezapour, R. P. Agarwal, *A new fractal-fractional version of giving up smoking model: Application of lagrangian piece-wise interpolation along with asymptotical stability*, Mathematics, **10** (2022), 1–31. 1

[13] C. L. Fischer Walker, M. J. Aryee, C. Boschi-Pinto, R. E. Black, *Estimating diarrhea mortality among young children in low and middle income countries*, PloS one, **7** (2012), 1–7. 1

[14] W. Gao, H. M. Baskonus, L. Shi, *New investigation of bats-hosts-reservoir-people coronavirus model and application to 2019-nCoV system*, Adv. Difference Equ., **2020** (2020), 11 pages. 1

[15] I. Goodfellow, Y. Bengio, A. Courville, *Deep learning*, MIT Press, Cambridge, MA, 2016. 1

[16] M. S. Hashemi, M. Inc, A. Yusuf, *On three-dimensional variable order time fractional chaotic system with nonsingular kernel*, Chaos Solitons Fractals, **133** (2020), 8 pages. 1

[17] R. Hilfer, *Applications of fractional calculus in physics*, World Scientific Publishing Co., River Edge, NJ, (2000). 1

[18] R. A. Khan, K. Shah, *Existence and uniqueness of solutions to fractional order multi-point boundary value problems*, Commun. Appl. Anal., **19** (2015), 515–525. 1, 4

[19] V. Lakshmikantham, S. Leela, *Nagumo-type uniqueness result for fractional differential equations*, Nonlinear Anal., **71** (2009), 2886–2889. 1

[20] S. Lane, D. Lloyd, *Current trends in research into the waterborne parasite giardia*, Crit. Rev. Microbiol., **28** (2022), 123–147. 1

[21] Y. A. Liana, F. M. Chuma, *Mathematical modeling of giardiasis transmission dynamics with control strategies in the presence of carriers*, J. Appl. Math., **2023** (2023), 14 pages. 1

[22] T. Mahmood, M. ur Rahman, M. Arfan, S.-I. Kayani, M. Sun, *Mathematical study of algae as a bio-fertilizer using fractal–fractional dynamic model*, Math. Comput. Simulation, **203** (2023), 207–222. 1

[23] W. S. McCulloch, W. Pitts, *A logical calculus of the ideas immanent in nervous activity*, Bull. Math. Biophys., **5** (1943), 115–133. 1

[24] S. C. Mpeshe, N. Nyerere, *A human-animal model of giardiasis infection in contaminated environment*, Int. J. Adv. Appl. Math. Mech., **8** (2021), 37–47. 1

[25] T. Nabil, *Krasnoselskii N-tupled fixed point theorem with applications to fractional nonlinear dynamical system*, Adv. Math. Phys., **2019** (2019), 9 pages. 2.4

[26] S. Osman, H. A. Togbenon, D. Otoo, *Modelling the dynamics of campylobacteriosis using nonstandard finite difference approach with optimal control*, Comput. Math. Methods Med., **2020** (2020), 12 pages. 1, 2

[27] I. Podlubny, *Fractional differential equations, mathematics in science and engineering*, Academic Press, New York, (1999). 1

[28] H. Qu, M. Ur Rahman, M. Arfan, G. Laouini, A. Ahmadian, N. Senu, S. Salahshour, *Investigating fractal-fractional mathematical model of Tuberculosis (TB) under fractal-fractional Caputo operator*, Fractals, **30** (2022), 14 pages. 1

[29] S. Qureshi, A. Atangana, *Fractal-fractional differentiation for the modeling and mathematical analysis of nonlinear diarrhea transmission dynamics under the use of real data*, Chaos Solitons Fractals, **136** (2020), 14 pages. 1

[30] S. Qureshi, A. Yusuf, A. A. Shaikh, M. Inc, D. Baleanu, *Mathematical modeling for adsorption process of dye removal nonlinear equation using power law and exponentially decaying kernels*, Chaos, **30** (2020), 9 pages. 1

[31] H.-O. Rashid, R. K. Yadav, H.-R. Kim, H.-J. Chae, *Er stress: Autophagy induction, inhibition and selection*, Autophagy, **11** (2015), 1956–1977. 1

[32] S. Rezapour, J. K. K. Asamoah, S. Etemad, A. Akgül, İ. Avcı, S. M. El Din, *On the fractal-fractional mittag-leffler model of a covid-19 and zika co-infection*, Results Phys., **55** (2023), 1–21. 1

[33] S. Rezapour, S. Etemad, İ. Avcı, H. Ahmad, A. Hussain, *A study on the fractal-fractional epidemic probability-based model of SARS-CoV-2 virus along with the Taylor operational matrix method for its Caputo version*, J. Funct. Spaces, **2022** (2022), 33 pages. 1

[34] K. Shah, M. A. Alqudah, F. Jarad, T. Abdeljawad, *Semi-analytical study of Pine Wilt disease model with convex rate under Caputo-Febrizio fractional order derivative*, Chaos Solitons Fractals, **135** (2020), 9 pages. 1

[35] G. Spiga, M. Spiga, *Two-dimensional transient solutions for crossflow heat exchangers with neither gas mixed*, J. Heat Transfer., **109** (1987), 281–286. 1

[36] S. A. Squire, U. Ryan, *Cryptosporidium and giardia in africa: current and future challenges*, Parasites Vectors, **10** (2017), 1–32. 1

[37] A. Sulemana, T. A. Paget, E. L. Jarroll, *Commitment to cyst formation in giardia*, Microbiology, **160** (2014), 330–339. 1, 2

[38] M. ur Rahman, *Generalized fractal–fractional order problems under non-singular Mittag-Leffler kernel*, Results Phys., **35** (2022), 15 pages. 1

[39] M. ur Rahman, A. Althobaiti, M. B. Riaz, F. S. Al-Duais, *A theoretical and numerical study on fractional order biological models with caputo fabrizio derivative*, Fractal Fract., **6** (2022), 1–15. 1

[40] A. Waldram, R. Vivancos, C. Hartley, K. Lamden, *Prevalence of giardia infection in households of giardia cases and risk factors for household transmission*, BMC Infect. Dis., **17** (2017), 1–7. 1, 2

[41] World Health Organization, *Global diffusion of eHealth: making universal health coverage achievable: report of the third global survey on eHealth*, World Health Organization, (2017). 1

[42] C. Yildiz, M. Heinonen, H. Lahdesmaki, *ODE2VAE: Deep generative second order ODEs with Bayesian neural networks*, Adv. Neural Inf. Process. Syst., **32** (2019). 1

[43] Y.-Z. Zhang, A.-M. Yang, Y. Long, *Initial boundary value problem for fractal heat equation in the semi-infinite region by yang-laplace transform*, Therm. Sci., **18** (2014), 677–681. 1